



Modeling and Experimental Efforts towards Robust Low-Cost Cruciform Canopy Control

Gregory M. Noetscher¹, Terrance Rose², and Keith Bergeron³
US Army Combat Capabilities Development Command Soldier Center, Natick, MA, 01760, USA

Over the years, precision guided cargo airdrop has taken many forms with most attempting to optimize payload delivery accuracy over all other variables. More recent developments have placed system cost and the ability to perform accurately in highly vertical drop environments as higher priorities, necessitating a departure from more traditional parafoil based vehicles. This work describes the numerical and experimental examination of a cruciform based cargo payload system in the context of modern operational considerations. The design process is holistic, making extensive use of a two-way fluid-structure interaction (FSI) model to characterize steady flight and coupling this with collection and analysis of tradition live drop test data to understand deployment dynamics and responses to environmental conditions. This has resulted in a system that has the potential to leverage existing concepts of operation and flight planning tools while extending operational and logistics support in real-world mission scenarios.

I. Nomenclature

AR	=	aspect ratio of cruciform canopy
Rs	=	suspension line ratio
L	=	cruciform canopy planform length
Ls	=	suspension line length
W	=	cruciform canopy center width
ψ	=	canopy heading
θ	=	canopy pitch or angle of attack

II. Introduction

Reliable precision delivery of essential supplies in remote and austere environments is a long standing topic of research within the U.S. Army [1] with solutions ranging from enhancements to traditionally ballistic systems [2] to high performance canopies optimized for high lateral standoff [3]. While all strive to provide the best solution for a given mission scenario, each cargo airdrop concept or configuration has trade-offs between cost and capabilities with manufacturing labor playing a significant factor in system cost. For this reason, interest in low cost systems with some degree of control authority has risen recently, with particular focus on cruciform parachute designs [4]-[9].

Moderate control of a cruciform geometry has been demonstrated in a variety of scenarios and formulations [9]-[10]. Corresponding simulation studies using various commercial or academic software packages have also been executed [11]-[12], providing insight into both the degree of controllability that may be achieved and the governing aerodynamics. While these studies have proven the concept of a steerable cruciform based system, no one solution has proven to be significantly better than another to warrant widespread adoption in the field, leaving the question of cruciform control open for debate.

The mechanism for control described in this research effort is depicted in Fig. 1. After initial deployment, the panels or ‘arms’ of the cruciform are arranged in a ‘pinned’ position, tying all panel corners together; in this configuration, the system is essentially acting as a traditional flat circular canopy, to fall in a predominantly vertical

¹ Senior Research Electrical Engineer, Airdrop Technology Team, AIAA Member.

² Mathematician, Airdrop Technology Team, AIAA Member.

³ Senior Research Aerospace Engineer, Airdrop Technology Team, AIAA Associate Fellow.

direction. Some side venting is achieved to reduce oscillatory behavior during flight. Upon actuation via a separate control line, one set of corners is released, enabling a venting of air between two adjacent parachute canopy panels. This venting action produces a translational component to the trajectory of the parachute, resulting in control of the direction of flight, while maintaining the majority of the original shape integrity and drag force.

Given the highly flexible nature of the problem at hand, the Arbitrary Lagrangian-Eulerian (ALE) formulation within LS-DYNA was deemed a viable simulation method. The numerical implementation and the resulting simulation data are presented below. Some preliminary experimental data is also provided with more detailed validation efforts planned at upcoming test events.

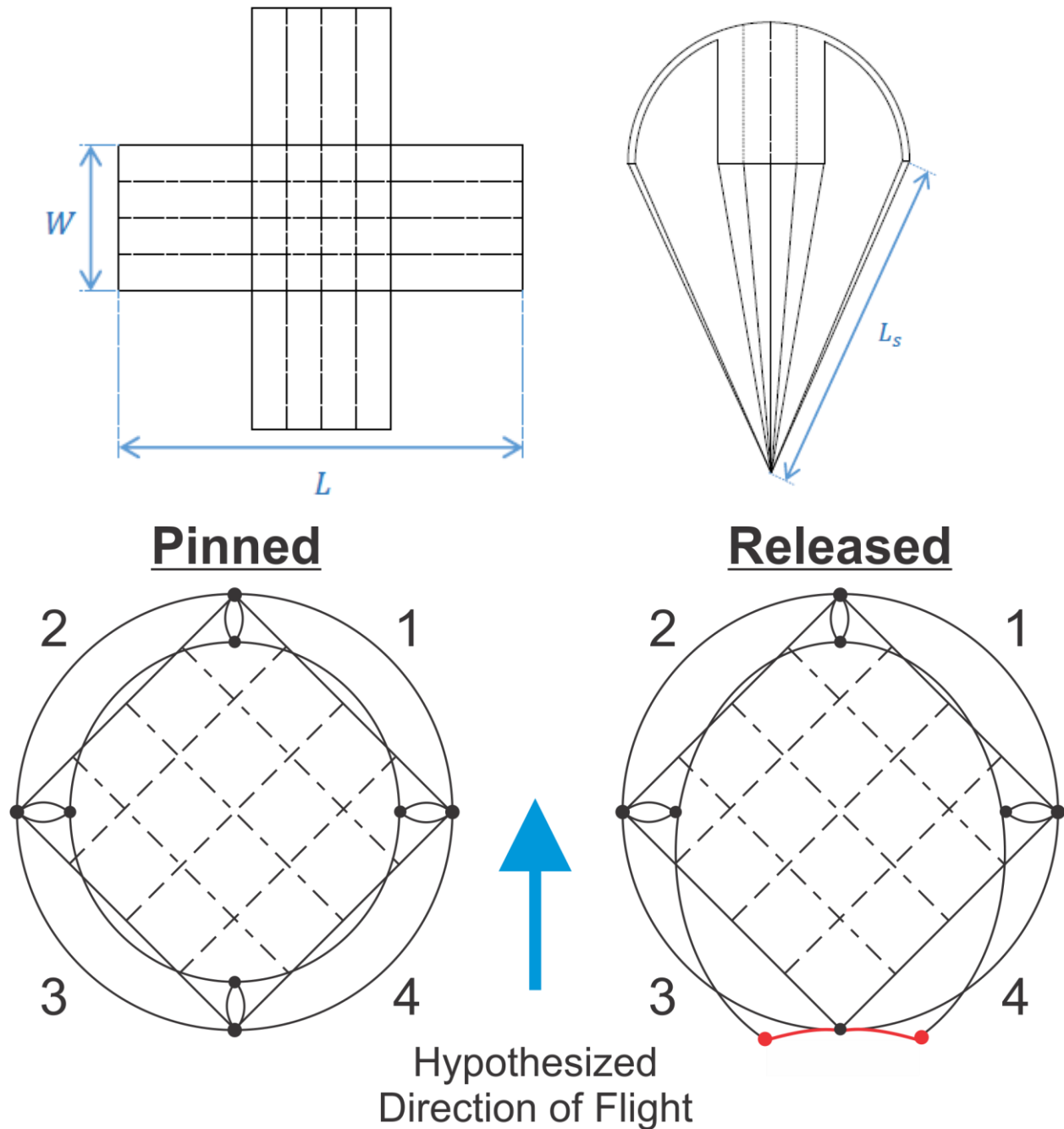


Figure 1: Top Left, planform geometry; Top Right, notional inflated shape with line length; Bottom Left, deployment configuration with the corners of all four parachute arms tied or 'pinned' together; Bottom Right, the fully actuated cruciform parachute with air venting occurring to induce a preferred direction of flight.

III. Methods

The methods employed in this project consist of both numerical and experimental components. Extensive simulations were conducted to examine the behavior of the parachute system in steady flight. While these simulations were executed without a payload, they provided a cost and time effective environment to iterate on design variables with excellent information on corresponding canopy drag force generated and stresses induced within the parachute structure. Toward the end of the simulation activities described below, experimental drop tests were conducted to validate the simulated configuration and to explore more dynamic behaviors, including opening shock. Each component of the design method is described in further detail below.

A. Simulation Setup

The computational cruciform parachute model was constructed in a manner similar to past LS-DYNA parachute modeling efforts considered by the US Army Combat Capabilities Development Command Soldier Center (CCDC-SC) [13]. A two-way fluid-structure interaction (FSI) model was created using the LS-DYNA Arbitrary Lagrangian-Eulerian (ALE) solver. The fluid is comparable to air flowing through a vertical column similar to a vertical tunnel and the structure is analogous to the parachute surfaces connected to suspension lines. These are coupled using `CONSTRAINED_LAGRANGE_IN_SOLID`, notably, the wind tunnel is the master, the parachute is the slave coupled as a Lagrangian porous solid to ALE material (`CTYPE = EQ.11`).

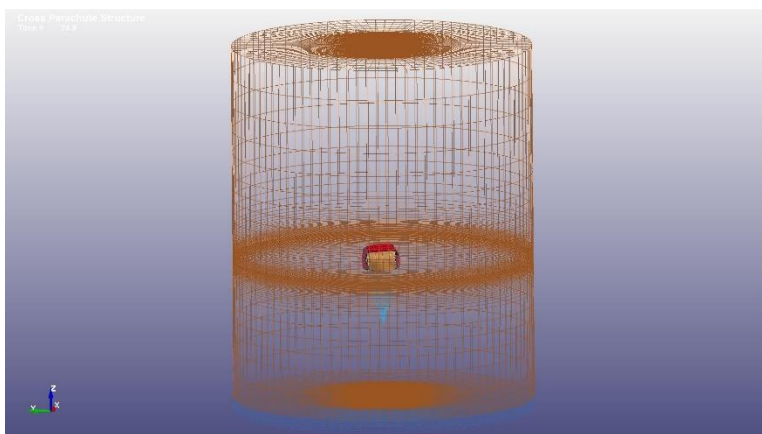


Figure 2: Above, shows the cruciform parachute within the vertical wind tunnel.

The virtual wind tunnel has a height of approximately 130 ft, radius of 100 ft, and was spatially discretized (meshed) using 360,000 `SOLID` elements using 370,000 nodes; this mesh is refined closer to the parachute and sparse near the walls. Nodes at the base are given an upward velocity comparable to parachute descent velocities seen in testing, which in this case is approximately 21 feet per second. This velocity is used by the `VZ` component in `INITIAL_VELOCITY` and the `BOUNDARY_PRESCRIBED_MOTION_SET`, notably, `z`-translational `DOF` (`DOF=EQ.3`), a load curve based in time, and a scale factor. The air represented is constructed using solid elements and `MAT_NULL` and with, most notable, mass density at sea level 1.22 kg/m^3 .

The parachute structure and dimensions were designed to be similar to the tested parachute. The parachute initial setup can be seen in Fig. 3 and deployed in Fig. 6. The parachute surfaces are built using `ELEMENT_SHELL` and `MAT_FABRIC` and suspension lines and limiters (which constrain the in-plane displacement of cruciform arms) are built using `ELEMENT_SEATBELT` and `MAT_SEATBELT`. The center area of the parachute is 9 ft by 9 ft, the four arms each measure 9 ft by 7 ft, divided into 1 in by 1 in elements, or 7900 elements and 8300 nodes. Each arm of the parachute is connected to five suspension lines, approximately 20 ft long. Each suspension line is constructed from one node on the parachute, one common node constrained in `x-y-z`, and one seatbelt element. To get the same overall length, slack length values were determined. Each limiter connects the node of one arm to its adjacent arm, using a single seatbelt element similar to the suspension lines, with a default slack length of 1 in. There were two forms of control using slack length of seatbelt elements. The first, seatbelt was change in the initial configuration file. The second, using the geometry from 0% configuration after it ran for 30 second real time, the parachute's nodal locations were used for the initial locations of the new case, such as 20%. In addition to limiters and suspension lines, seatbelt

elements were used to reinforce the parachute edges and surfaces, similar to stitching used during parachute manufacturing.

Parachutes deployment depends on many factors and interactions and is beyond the scope of the present work. Since the focus of this paper is controlling the parachute after inflation and during flight, the start of the simulation is very different than the experimental drop tests, and while initial conditions matter, our focus is after parachute reaches a steady state. To start the simulation, the virtual wind tunnel is allowed to reach proper velocity, as described above with INITIAL_VELOCITY and BOUNDARY_PRESCRIBED_MOTION_SET. The parachute surfaces are constrained against translational motion in the local x-y-z directions for 0.8 seconds using BOUNDARY_SPC_SET_BIRTH_DEATH, which was found by trial and error, providing sufficient pressure on the parachute to avoid deflation. In addition to a translational constraint and in an effort to minimize perturbations of initial conditions, parachute nodes along the x- and y-axis are translationally constrained to their respective axis using the same keyword.

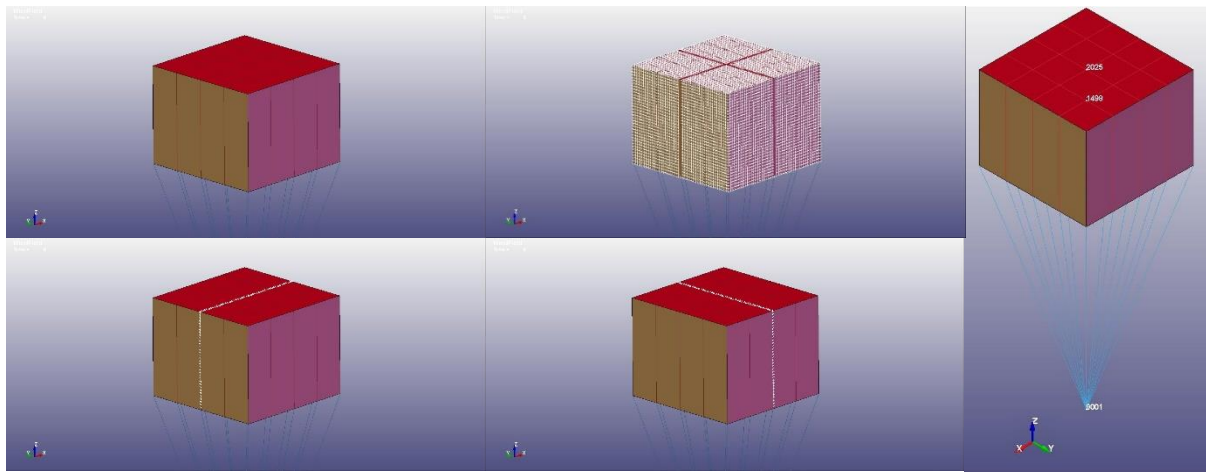


Fig. 3 Top-left, initial deployment of the parachute; Top-middle, nodes translationally x-y-z constrained for 0.8 seconds; Bottom-left, nodes are constrained to the x-axis for 5 seconds; Bottom-middle, nodes are constrained to the y-axis for 5 seconds; Right, show nodes used for heading and pitch calculations.

Simulations were completed on a distributed cluster operated by The U.S. Army Engineer Research and Development Center (ERDC) through the DoD High Performance Computing Modernization Program (HPCMP). For 30 second of real time simulation or problem time, there were a total of 555,556 cycles, for a total 20 hours and 25 minutes of CPU time. These were distributed on 8 parallel processors using LS-DYNA 971.R7.1.2 double precision. Each tenth of a second of problem time produces roughly 70MB of combined d3plot and binout data.

B. Experimental Setup

Full scale drop tests of the system depicted in Fig.1 were conducted on November 9th, 2017 at a commercial drop zone in Eloy, Arizona. The system was deployed multiple times during the course of a single day from a Skyvan aircraft at an airspeed of 110 knots indicated. The payload weight was 150 lbs. and the total rigged weight, including the parachute, Airborne Guidance Unit (AGU) and payload was 205 lbs. The system was released from an altitude of approximately 6,500 ft Mean Sea Level (MSL); the drop zone altitude was 1,549 ft, leaving 4,051 ft of altitude for flight and maneuvers.

The AGU mentioned above is a control system used on the Joint Precision Airdrop System (JPADS) [1] that houses motors, gearboxes, sensors (GPS, inertial measurement unit, etc.) and a microprocessor that is capable of executing autonomous flight software. In this scenario, one motor was attached to a control line that released the corners of two cruciform arms as described in Fig. 1. The AGU also enabled manual flight control from an independent ground station via a radio frequency communications channel and recorded all flight data for post-processing.

The total stroke available to the motor was 38 inches; this implies that the control line attached to the corners of the cruciform arms could be extended outward by 38 inches. The arms of the cruciform were attached to each other via a ‘limiter’ or piece of ½” tubular webbing to help maintain parachute shape, so in practice, this full stroke was likely not reached.

Throughout the course of each flight, the parachute was deployed with 0% of the total stroke extended. Once stable, the control line was extended in either 10% or 25% stroke increments with a short period between each release

to reach a semi-stable flight condition. System configurations for 0%, 50% and 100% stroke are shown below in Fig. 4

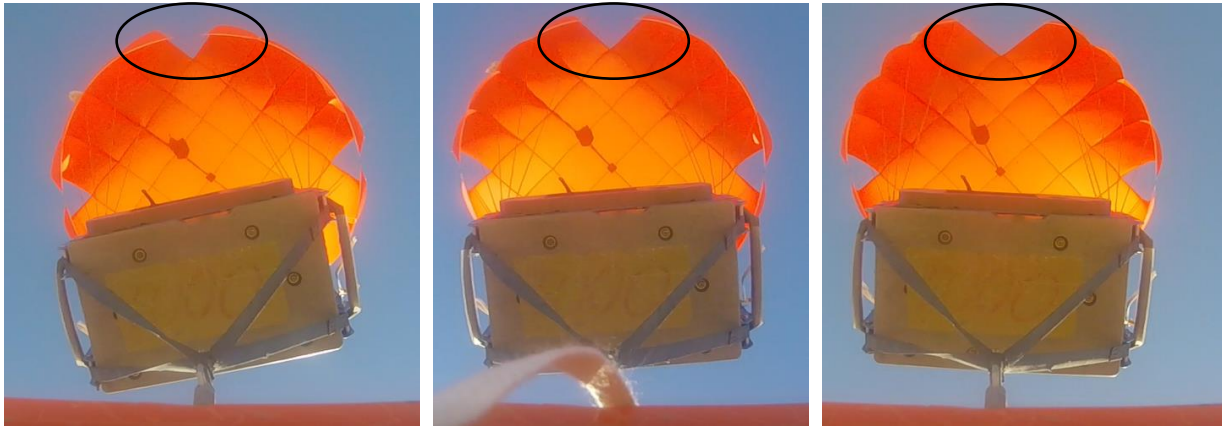


Fig. 4 Left, deployment configuration with 0% stroke extended and the actuated corners tied together; Center, approximately 50% of total stroke deployed; Right, 100% of stroke extended to produce the fully deployed configuration. In all images, the actuated corners are at the top of the figure.

IV. Results

A. Simulation Results

LS-PrePost and MATLAB were used for post analysis. While the goal of these simulations is to rapidly model ideas, the model must produce results which correlate to the real world. There was an effort to create a motor actuated equivalent model which could provide stroke increments using a combination of BOUNDARY_PRESCRIBED_MOTION_NODE and ELEMENT_SEATBELT_SLIPRING, but for this paper, new simulations were executed with varying slack lengths. Six models were created with a limiter's slack length varying from 0, 20, 40, 60, 80, and 100%.

When looking into building a closed-loop control for this type of parachute, there are two important figures of merit: heading, ψ , and pitch, θ or angle of attack. The heading was determined using a node on the parachute surface and its location relative to the center most node on the surface. The pitch was determined using the same center most node on the surface and the point where all suspension lines meet at the confluence point.

In Fig. 5, the heading and pitch are shown for varying simulated actuations in stroke. It is interesting to note that the parachutes all rotate in a similar direction. Since there is no control algorithm, there is reason to suggest, as the stroke increases from 40% to 100%, interactions with the canopy and fluid flow may provide a controllable turn rate. Since actuations of 0% to 20% provide no to little changes in flow, other factors may lead to some randomness. The relatively small heading changes seen in the simulations qualitatively match the behavior exhibited during drop tests, providing some initial qualitative verification of the simulated dynamics.

The pitch in Fig. 5 provided more distinct characteristics. As the opening between arms increases, more air escapes, creating a driving force in the opposite direction. While the next step is to run the simulations longer, after deployment, the pitch can be correlated with the different strokes. This can also be seen in Fig. 6, the view is looking at the parachute through the x-y plane, and any pitch can be seen relative to the center of the parachute and the node where all suspension lines meet. The parachute is shift slightly for the 0% case but is more distinctive in the 100% case. There is also a pressure change seen on the surface of the parachute, utilizing Fringe Component tools in LS-PrePost.

The simulation environment allows for close examination of forces at particular regions as well as visualization of particular flow quantities of interest. Examples of these analysis options are shown in Fig. 7. The top portion of the figure shows how the force located at the parachute confluence point (where a payload would be attached) develops as the simulation progresses. After an initial period of extreme instability, the force settles to a quasi-steady state value. The lower left portion shows a representative visualization of velocity isosurfaces encapsulating and flowing past the parachute while the lower right displays streamlines. This type of analysis enables determination of shedding behavior.

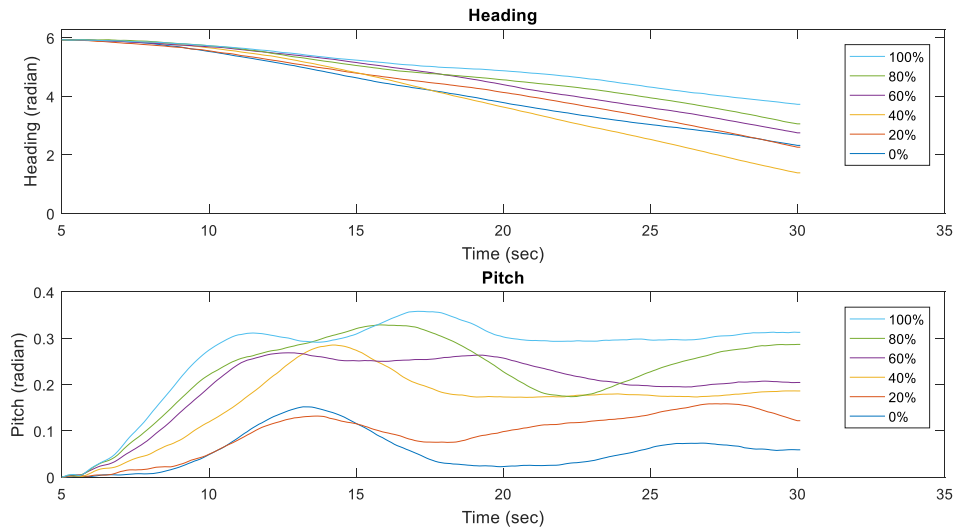


Fig. 5 Simulated heading and pitch at varying actuation as a percentage of stroke.

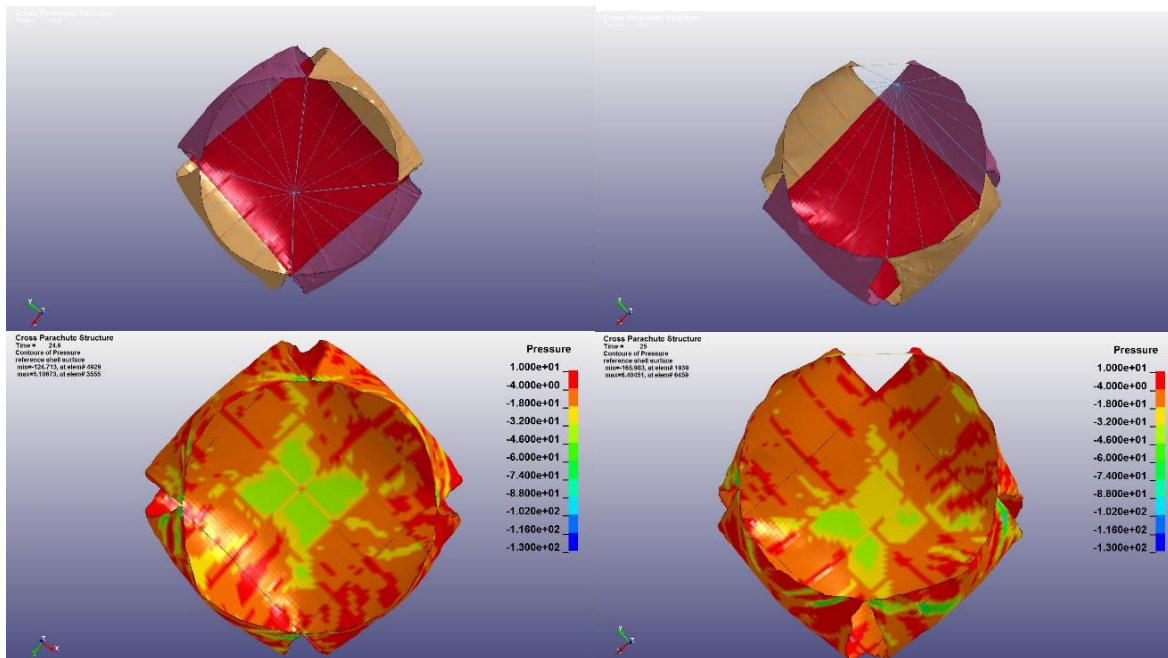


Fig. 6 Top-left, simulation equivalent to deployment configuration with 0% stroke extended and the actuated corners tied together, as viewed from below; Top-right, 100% of stroke equivalent extended to produce the fully deployed configuration, as viewed from below; Bottom-left pressure distribution for 0% stroke extended; Bottom-right pressure distribution for 100% stroke extended.

B. Experimental Results

Plots of the typical altitude and descent velocities are shown in Fig. 8 below. The average descent velocity after deployment and steady flight is attained is approximately 22.2 ft/s. This matches the simulated flow velocity of 21 ft/s quite well.

The data depicted in Fig. 9 below is from the first flight of the system, which was actuated in stroke increments of 25%. Individual stroke actuations below 50% produced relatively little control of the system heading with the measurements indicating a rotating behavior. However, once 50% of stroke was achieved, some stability of heading

was evidenced, shown in Fig. 9 at approximately 68.4 seconds. At this point, heading measurements cease changing rapidly as the flow of air from the vent opening overcame the rotating inertia and propelled the system

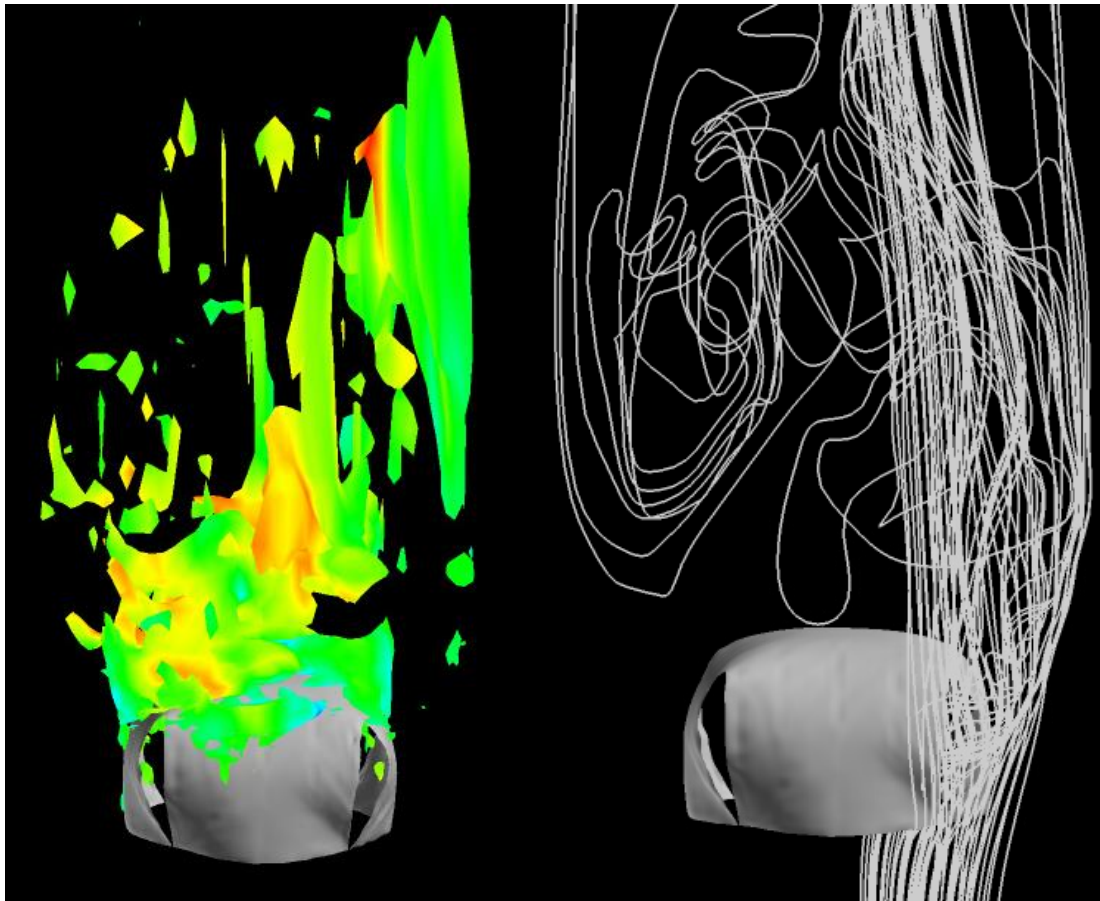
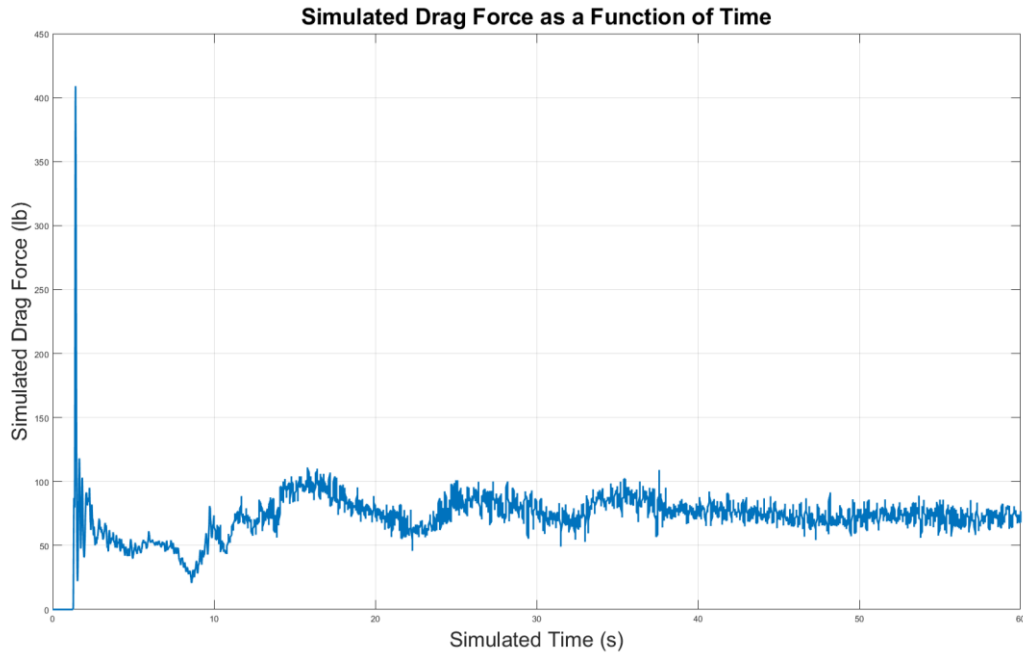


Fig. 7 Top, simulated drag force as a function of numerical time; Bottom, representative plots of velocity isosurfaces (let) and streamlines (right)

A second instance of controlled heading can be seen at about 80 seconds of flight. Here, the motor was actuated from 0% to 100% of stroke, inducing what appears to be system directionality along a stable heading.

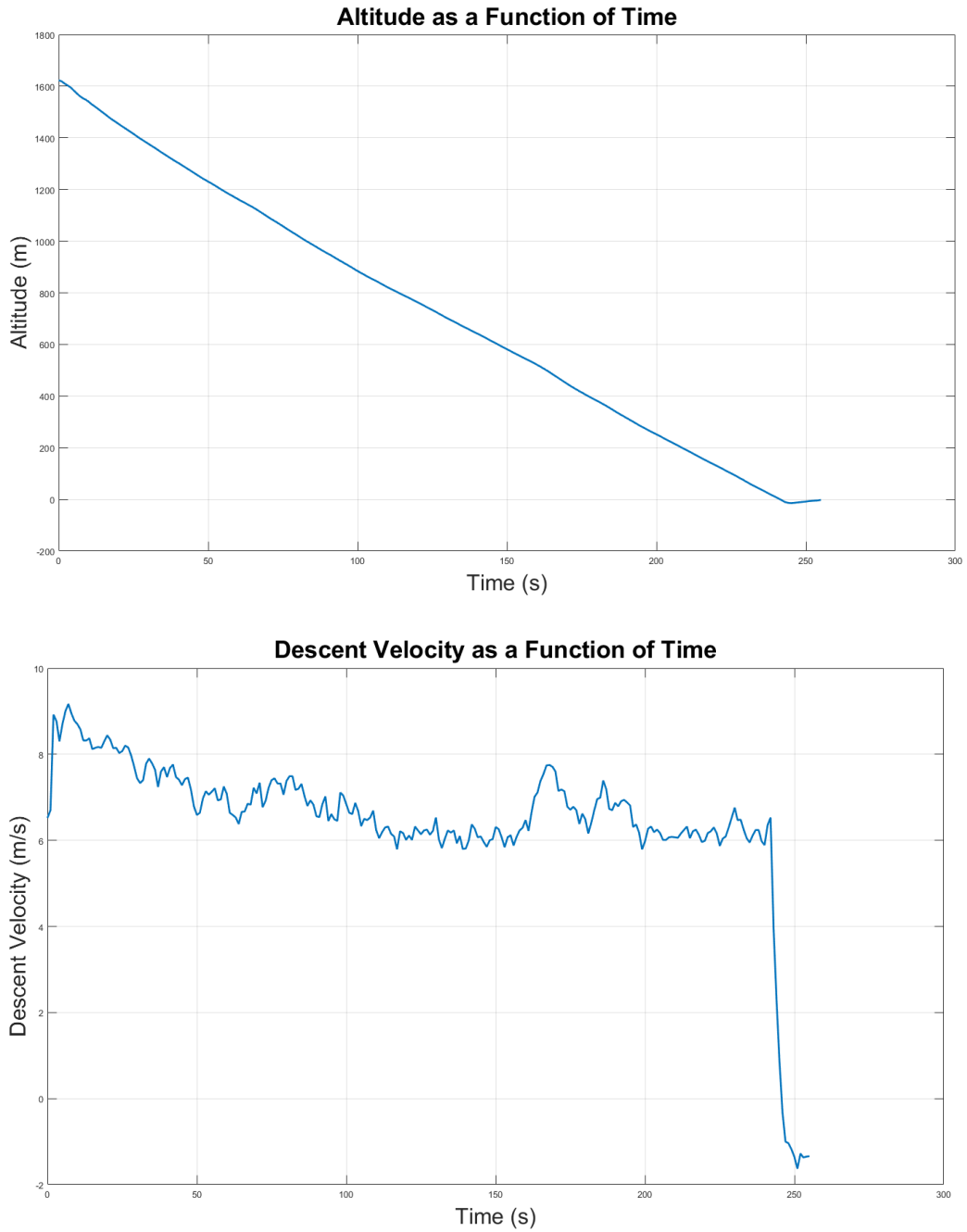


Fig. 8 Top, the motor position is shown with actuations of 25%, 50%, 75% and 100% stroke length. Bottom, the system's heading as derived from GPS data. During the transition from 0% to 100% of stroke at approximately 800 seconds, a degree of heading control is achieved.

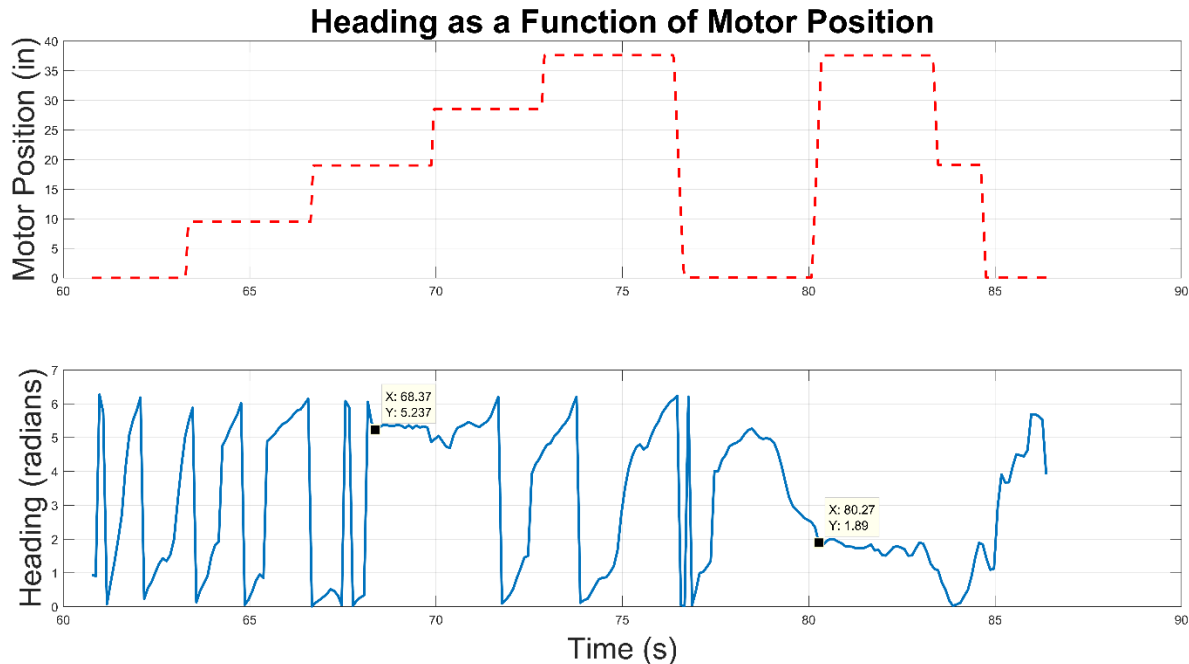


Fig. 9 Top, the motor position is shown with actuations of 25%, 50%, 75% and 100% stroke length. Bottom, the system's heading as derived from GPS data. During the transition from 0% to 100% of stroke at approximately 800 seconds, a degree of heading control is achieved.

V. Conclusions

This paper presents a review of efforts by the U.S. Army Combat Capabilities Development Command Soldier Center toward the goal of constructing a cost effective, guided parachute system based on a cruciform canopy. Simulation and experimental results were presented, describing the execution of the system design and experimental characterization processes. The system has been shown to exhibit a certain amount of control when particular canopy structures are deflected, while also demonstrating a soft landing. Future work in this area is planned to include the ability to quickly penetrate high altitude wind conditions via drogue fall and other control mechanisms designed to stabilize system heading.

Acknowledgments

The authors wish to thank Mr. Frank Deazley, President, Aerial Delivery Solutions, LLC. of Kissimmee, FL for his assistance in construction of the experimental cruciform system, execution of their testing and ideas related to cruciform control discussed herein. The authors would also like to acknowledge the DoD High Performance Computing Modernization Program for providing the computational resources to complete the simulations.

References

- [1] Benney, R., McGrath, J., McHugh, J., Noetscher, G., Tavan, S., and Patel, S., "DOD JPADS programs overview and NATO activities," 19th AIAA Aerodynamic Decelerator Systems Technology Conference and Seminar, 2009, p. 2576.
- [2] Dellicker, S., Benney, R., and Brown, G., "Guidance and control for flat-circular parachutes," *Journal of Aircraft*, Vol. 38, No. 5, 2001, pp. 809–817.
- [3] Carter, D. et al, "Band-limited guidance and control of large parafoils," 20th AIAA Aerodynamic Decelerator Systems Technology Conference and Seminar, 2009, p. 2981.
- [4] Division, A. S., "Technical Evaluation of the French Cross Parachute," Tech. rep., Air Force Systems Command Technical Memorandum, ASNM-TM-6321.
- [5] Niccum, R. J., Haak, E. L., and Gutenkauf, R., "Drag and stability of cross type parachutes," Tech. rep., DTIC Document, 1965.
- [6] Foughner Jr, J. T. and Alexander, W. C., "Wind tunnel tests of modified cross, hemisflo, and disk-gap-band parachutes with emphasis in the transonic range," 1974.

- [7] Jorgensen, D. and Cockrell, D., “Aerodynamics and performance of cruciform parachute canopies,” 7th Aerodynamic Decelerator and Balloon Technology Conference, 1981, p. 1919.
- [8] Jorgensen, D. S., Cruciform Parachute Aerodynamics, Ph.D. thesis, University of Leicester, 1982.
- [9] Potvin, J., Papke, J., Brighton, E., Hawthorne, T., Peek, G., and Benney, R., “Glide Performance Study of Standard and Hybrid Cruciform Parachutes,” 17th AIAA Aerodynamic Decelerator Systems Technology Conference and Seminar, 2003, p. 2160.
- [10] Fields, T. D., and Yakimenko, O. A., “Development of a steerable single-actuator cruciform parachute,” *Journal of Aircraft*, 2017, pp. 1–9. doi:10.2514/1.C034416.
- [11] Brocato, B., Esteve, L., Garcia, D., Manglano, C., Peek, G., Potvin, J., Stein, K., Benney, R., Alamat, R., and Little, J., “Experimental study of fluid-structure interactions on a cross parachute-Comparison of wind tunnel data and drop data with CFD predictions,” 15th Aerodynamic Decelerator Systems Technology Conference, 1999, p. 1737.
- [12] Fagley C.P., Seidel J., McLaughlin T.E., Noetscher G., Rose, T.M., “Computational study of air drop control mechanisms for cruciform parachutes”, 24th AIAA Aerodynamic Decelerator Systems Technology Conference, AIAA AVIATION Forum, (AIAA 2017-3541) <https://doi.org/10.2514/6.2017-3541>
- [13] Tutt, B., Roland, S., Charles, R., Noetscher, G., “Development of parachute simulation techniques in LS-DYNA,” 11th International LS-DYNA User’s Conference, Dearborn, MI, June 2010.